Extended Data

Model evaluation for different historical periods

For the historical period (1901-2014) using observation-based climate data, the modelled leaf area index (LAI), gross primary productivity (GPP) and aboveground carbon (ABC) are evaluated against satellite-based dataset (Extended Data Figs.1-3). The modelled ecosystem-level BVOC emissions are evaluated with observations from the available literature (Extended Data Table 1).

The modelled gross primary productivity (GPP) has been evaluated against the OCO-2-based SIF GPP product (GOSIF)[1], and the mapping of multiple-year averages show general agreements in spatial patterns (Extended Data Fig. 1a, b). The modelled GPP is higher than estimates based on GOSIF in the southern boreal forest and also in terms of areal average. The modelled interannual variability of annual areal averaged GPPs correlates well with the observations based on GOSIF (Extended Data Fig. 1c).

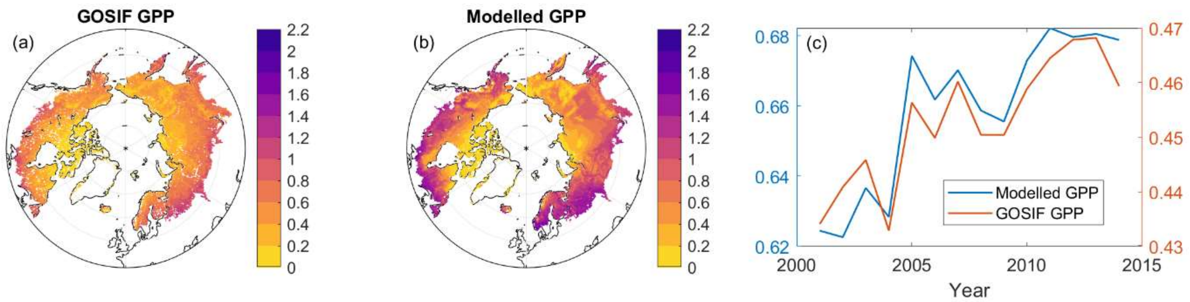

Extended Data Figure 1. Comparing the modelled annual gross primary productivity (GPP) with the GOSIF GPP product. (a) Annual GOSIF-based GPP averaged over the period of 2001-2014; (b) LPJ-GUESS modelled annual GPP averaged over the period of 2001-2014; (c) the timeseries of annual, areal average of GPP (KgC/m2) over the study domain (including tundra and boreal regions).

The modelled LAI averaged over June, July and August are compared with estimates from the GIMMS LAI3g[2] product over the same period (Extended Data Fig. 2). We find that the modelled spatial patterns of LAI are similar to GIMMS LAI3g though the absolute differences (Extended Data Fig. 2c) show that the model tends to overestimate LAI in some of tundra regions, such as in north America, Norway and northern parts of Finland and small regions of Siberia. In contrast, slight underestimations are found in the southern part of boreal region.

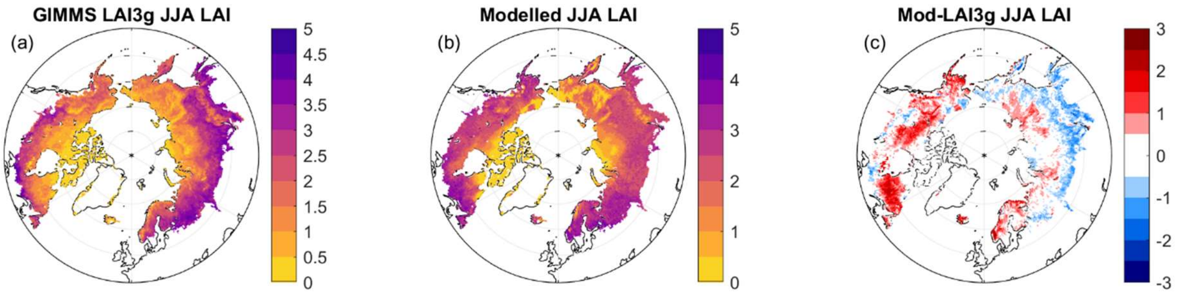

Extended data Figure 2. Comparing the modelled leaf area index (LAI) over the growing season (June, July and August, JJA) with the GIMMS LAI3g product over the period 1982-2011. (a) GIMMS LAI3g-observed averaged LAI in JJA; (b) LPJ-GUESS modelled LAI in JJA; (c) the difference in the modelled JJA LAI between the modelled and the GIMMS LAI3g product.

The modelled aboveground carbon pool (i.e., leaf and stem carbon in vegetation) is compared with estimates from a vegetation optical depth (VOD)-based product[3]. The overall spatial patterns are captured by the model (Extended Data Fig. 3a, b), and though there is an overestimation of areal averages of aboveground carbon from our model, the increasing trends are well represented (Extended Data Fig. 3c).

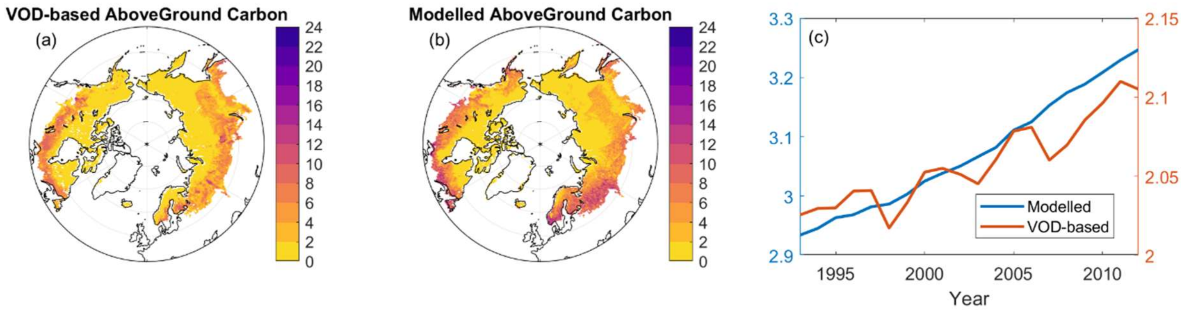

Extended Data Figure 3. Comparing the modelled annual aboveground biomass carbon (ABC, KgC m^{-2}) with vegetation optical depth (VOD)-based ABC product. (a) VOC-based ABC averaged over the period of 1993-2012; (b) LPJ-GUESS modelled aboveground carbon (including biomass from leaf and stem) averaged over the period 1993-2012; (c) the timeseries of areal averaged ABC over the study domain (including tundra and boreal regions).

The above comparison of modelled and regional estimates of GPP, LAI and ABC show that the model can generally capture the spatial and temporal changes of these variables, though with some overestimations of GPP and ABC for southern boreal regions and of LAI for the tundra region.

The modelled ecosystem-level isoprene and monoterpene fluxes are compared with the published values from different ecosystems (Extended Data Table 1), which show that the model produce fluxes of similar magnitudes to the observed emissions. We note, however, that an exact comparison was not possible since the LPJ-GUESS model runs at a spatial resolution of 0.5 degrees, and although we used the output from the nearest gridcells with a similar dominant vegetation type as observed at the sites, there could still have differences in terms of overall vegetation composition and microclimatic conditions.

Extended Data Table 1 Ecosystem-level BVOC evaluation. The modelled values from the nearby gridcell were selected and the modelled units were converted to the same one as the one in the literature. Noted: only ecosystem-level observations were extracted from the literature. Dom.: dominated; MT: monoterpenes; ISO: isoprene

Ecosystem types	**Location**	**Dom. Species**	**Time**	**Compounds**	**Units**	**Observed**	**Modelled**	**Refs**
Boreal forest	Siberian larch tree	*Larix cajanderi*	Jun, 2009 Jul, 2009	MT MT	mgC/m^2/d	3.3±2.9 2.4±1.6	2.0 2.4	[4]
	Scots pine	*Pinus sylvestris*	Mar, 2010-2013 Apr, 2010-2013 May, 2010-2013 Jun, 2010-2013 Jul, 2010-2013 Aug, 2010-2013 Sep, 2010-2013 Oct, 2010-2013 Nov, 2010-2013 Dec, 2010-2013	MT	mgC/m2/m	10.87 27.44 85.08 114.35 163.07 103.98 57.18 30.72 6.63 7.56	6.82 23.40 54.99 75.96 111.15 77.53 42.97 24.18 15.73 9.33	[5]
Tundra upland	Greenland tundra	*Cassiope tetragona*	Aug, 2009	ISO MT	µgC/m2/h	1.38 21.54	0.014 0.014	[6]
	Alaska tundra	*Salix pulchra*	Jun-Jul 2005,2010&2011	ISO	µgC/m2/h	Up to 1200	63.2	[7]
	Alaska tundra	Tussock tundra	Summer, 2018&2019	ISO MT	µgC/m2/h	0.2-225 <1	0.2-118.8 0.34-4.81	[8]
Boreal wetland	Dry hummocks	Shrub and mosses	July, 2007	ISO	µgC/m2/h	24.5	85	[9]
	Boreal fen	*Sphagnum* mosses and sedges	July, 2007	ISO	µgC/m^2/h	186-220	198	[10]
	SubArctic fen	Graminoid	2006	ISO	µgC/m^2/h	Up to 1385	439	[11]
Tundra wetland	SubArctic fen	Graminoid	Jul, 2018 Jul, 2018	ISO MT	µgC/m^2/h	310 14	330 14	[12]

CMIP6 and predicted future climate change

We present details of the selected future emission scenarios and included general circulation model (GCM) in Extended Data Table 2. The design and description of the CMIP6 experimental protocol can be found in Eyring, et al. [13] and the outputs from these models were downloaded through ESGF (https://esgf-node.llnl.gov/search/cmip6/) for the period 1901-2100 (Date of access: Sep-2020). The climatology of the CRU-NCEP and CMIP6 datasets over the period 1985-2014 was calculated, and the monthly biases between CRU-NCEP and each CMIP6 model data were calculated. The biases were corrected to each climate field for the whole future period (2015-2100). The bias-corrected temperature, precipitation and radiation were used to drive the LPJ-GUESS simulation over the future period. The anomalies in Extended Data Fig. 3 show that over the study region, the predicted temperature increase can be up to 12 °C, the annual precipitation increase can be up to 250 mm yr^{-1} and the annual radiation show both increases and decreases. There is a general negative correlation between the changes in temperature and annual radiation. All of these 15 scenarios show that this region could become warmer and wetter, with a large range of responses between different CO_2 emission scenarios.

Extended Data Table 2 Overview of the selected future emission scenarios from CMIP6 and the general circulation model included in this study.

Scenario names	**Shared Socioeconomic Pathways (SSPs)**	**Climate forcing levels**	**Included general circulation model (GCMs)**
SSP585	SSP5	RCP8.5	CanESM5, MRI-ESM2-0, GFDL-ESM4
SSP370	SSP3	RCP7.0	CanESM5, MRI-ESM2-0, GFDL-ESM4
SSP245	SSP2	RCP4.5	CanESM5, MRI-ESM2-0, GFDL-ESM4
SSP126	SSP1	RCP2.6	CanESM5, MRI-ESM2-0, GFDL-ESM4
SSP119	SSP1	RCP1.9	CanESM5, MRI-ESM2-0, GFDL-ESM4

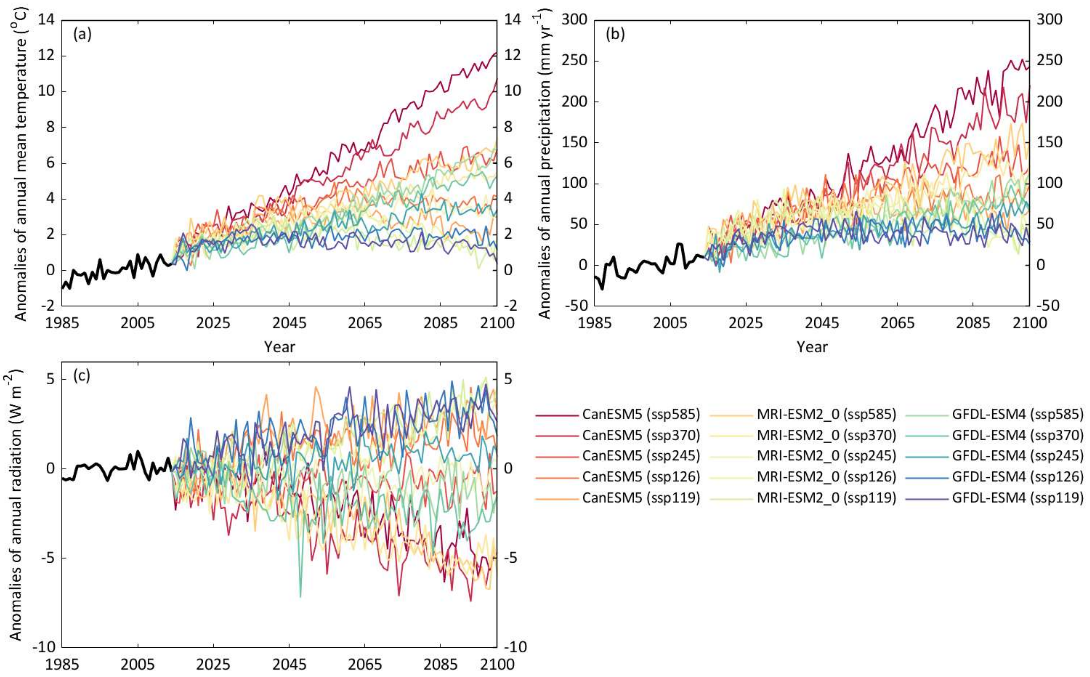

Extended Data Figure 4 Anomalies of annual mean temperature (a), precipitation (b) and surface shortwave radiation (c) over 1985-2100. The period 1985-2014 has been used as the base line to calculate anomalies.

Total isoprene and monoterpene emissions

The distribution of significant trends in isoprene emissions reveals that a larger area displays a positive trend in isoprene emission in predictions with greater levels of climate change, which is however not the same for monoterpene emissions (Extended Data Fig. 5). For monoterpenes, the higher CO_2 emission scenarios (such as SSP585) together with warmer climate conditions result in an increased area with significant negative trends, and a decrease in area with positive trends.

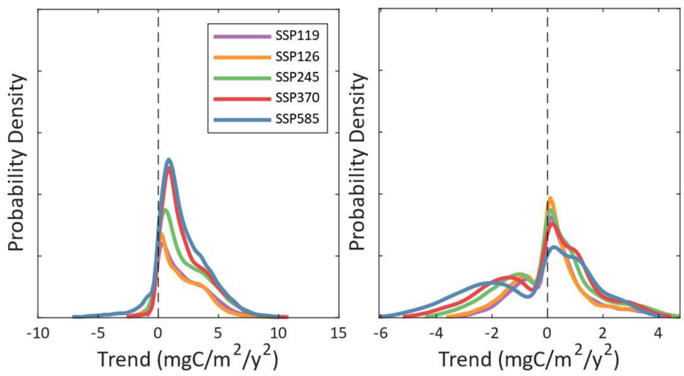

Extended Data Figure 5. Probability density of annual isoprene (left) and monoterpene (right) emission trends. The trends were calculated based on the averaged emissions over 3 GCMs under each SSP, and only significant trends (Mann-Kendall trend test, $p<0.05$) are shown and included in plot.

The modelled latitudinal fractions of LAI, isoprene and monoterpene emissions for each PFT are shown in Extended Data Fig. 6. During the historical period 1971-2000, there are no emerging temperate evergreen species (represented by PFTs TeBE and TeNE in this region), but these two PFTs has started to appear in the future period 2071-2100 in the CanESM5 SSP585 scenario. The modelled changes in LAI, annual isoprene and monoterpene emissions (Extended data Fig. 6 b, d, f) show that: (1) in the high Arctic (north of 70 °N), there are large increases in the abundance of different heights of shrubs, cold grass (C3G) as well as boreal needle-leaved trees. The isoprene emissions increases are mainly contributed by the emissions from GRT, SPDS, as well as different boreal tree PFTs. The increases of monoterpene emissions in this region result mainly from emissions from boreal needle-leaved tree PFTs. (2) in the low Arctic and boreal region, there are widespread increases of IBS and TeBS (mainly in replacing of BNE and BINE, see Extended Data Fig. 6b), which result in a large increase of isoprene emissions from these two new, dominant PFTs. The increase of these two PFTs also contributes to a slight increase of monoterpene emissions, but the PFTs they replace, i.e., BNE and BINE, show large decreases, leading to a net decrease in monoterpene emission for these southern latitudinal bands.

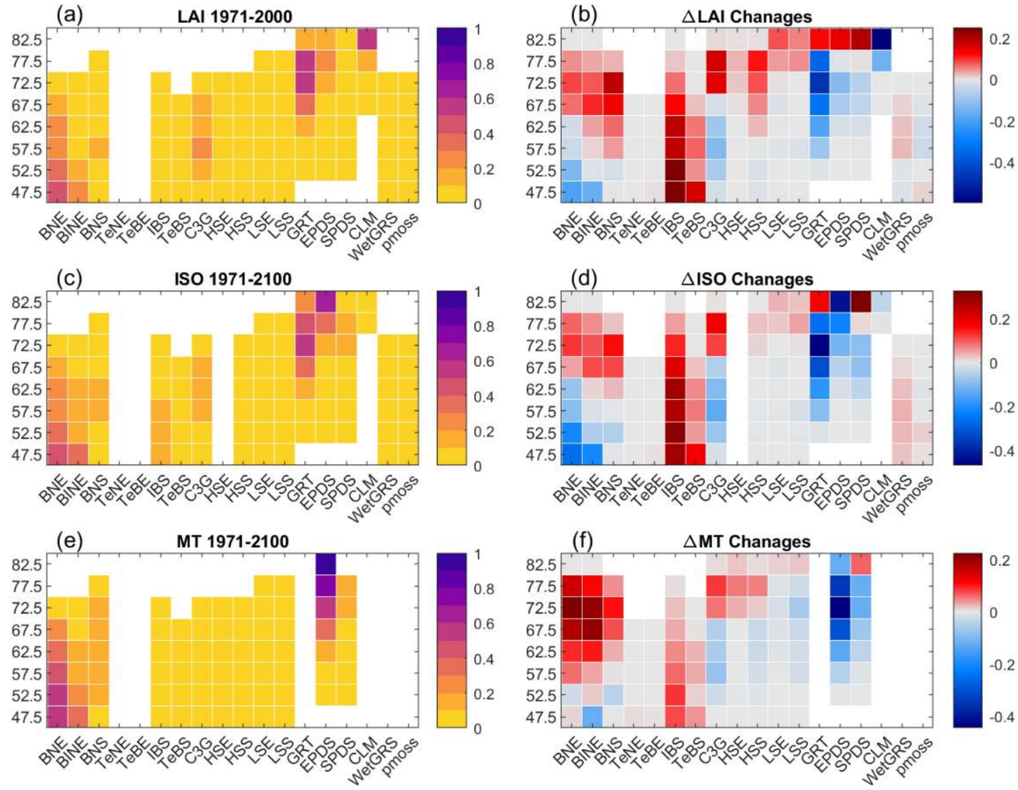

Extended Data Figure 6. Latitudinal fractions of leaf area index (LAI), annual isoprene (ISO) and annual monoterpene (MT) emissions for each modelled plant functions types (PFT, on the x-axis). The fractions of all PFTs within each latitudinal band add up till 1. The left column shows the modelled LAI, ISO and MT in latitudinal fractions for the period 1971-2000, and the right column shows the corresponding changes between 2071-2100 and 1971-2000. The future run was taken from CanESM5 SSP585. BNE: Boreal needle-leaved evergreen; BINE: Boreal shade-intolerant needle-leaved evergreen; BNS: Boreal needle-leaved summergreen; TeNE: Temperate needle-leaved evergreen; TeBE: Temperate broad-leaved evergreen; C3G: Cool grass; HSE: High shrubs evergreen; HSS: High shrubs summergreen; LSE: Low shrub evergreen; LSS: Low shrub summergreen; GRT: Graminoid and forb tundra; EPDS: Evergreen prostrate dwarf shrub; SPDS; Summergreen prostrate dwarf shrub; CLM; Cushion forb, lichen and moss; WetGRS: flood-tolerant grass; pmoss: peatland moss.

Factorial runs

Driven by climate data from CanESM5 SSP119 and CanESM5 SSP585, different factorial experiments are implemented (See Extended data Table 3). The associated effects are calculated as the differences between two runs.

Extended Data Table 3 Overview of factorial experiments conducted with LPJ-GUESS following CanESM SSP119 and SSP585.

Names of different runs	CO_2 inhibition	CO_2 fertilization of photosynthesis	CC-induced Vegetation Changess*	Nitrogen (N) limitation	CC impacts on BVOC productions*	Effects to analyse for 2015-2100
Standard run	Yes	Yes	Yes	Yes	Yes	Full Set
noCO_2inhibition	No	Yes	Yes	Yes	Yes	CO_2 inhibition = Standard run - noCO2inhibition
noCO_2	No	No	Yes	Yes	Yes	CO_2 fertilization = noCO_2inhibition – noCO_2
noNlim	Yes	Yes	Yes	No	Yes	N limitation = Standard runs – noNlim

noVegDym	Yes	Yes	No	Yes	Yes	Vegetation changes = Standard run-noVegDym

*CC: Climate change

TM5 modelled cloud condensation nuclei

The modelled cloud condensation nuclei (CCN) at 1.0% supersaturation from standard, noVegDym and noCO2Inhibition runs are further compared below. CCN (1.0%) roughly represents the number concentration of particles larger than 50 nm in diameter, so it is sensitive to new particle formation and growth which are affected by the gas precursors ELVOCs (extreme low volatile organic compounds) and SVOCs (semi-volatile organic compounds)[14]. Extended Data Figure 7 shows that a northward shift of CCN (1.0%), indicating potential more clouds at high latitude and less at mid latitude. This could result in global warming effect since less shortwave radiation is reflected by the same amount of clouds at high latitude compared to that at mid latitude, which is similar with the mid-latitude cloud reflectance feedback (Fig. 6 in [15]).

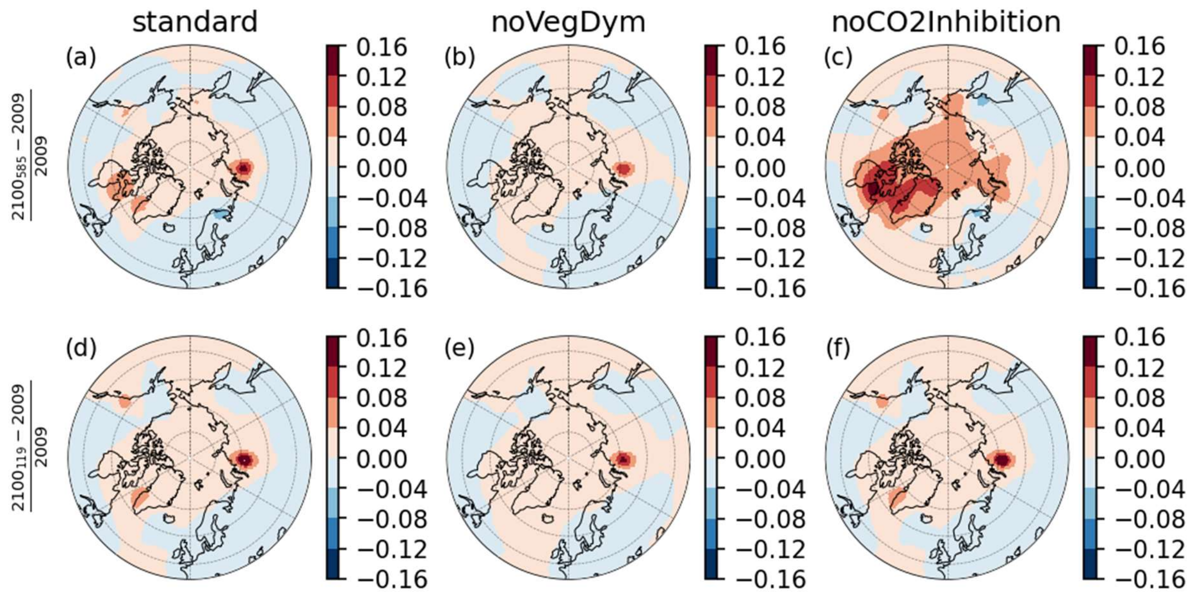

Extended Data Figure 7 CCN concentration at 1.0% supersaturation in the unit of [# cm-3] and two factorial experiments, namely noVegDym and noCO2Inhibition. The top and low panels show the results driven by CanESM5 SSP585 and CanESM5 SSP119, respectively.

Model uncertainties

Uncertainties in modelled vegetation changes

The northward shifts of woody plants as well as changes to PFT compositions simulated by LPJ-GUESS consider PFT competition and PFT responses to changing climatic and environmental conditions, including soil conditions and nutrients availability. Migration and establishment rates may be overestimated as constraints such as seed dispersal have not been accounted for in the model[16]. However, tree demography and competition rather than seed dispersal have been shown to be more important in limiting vegetation shifts in the Alps[17]. Our modelled vegetation responses to climate (e.g., replacement of evergreen trees with deciduous trees, shrubification and northward movements of evergreen trees) are consistent with experimental evidences[18] and other modelling studies[4,19].

Uncertainties in modelled aerosol changes

Other uncertainties of the TM5 model itself also applied to this study. For example, the wet removal of aerosol particles may be overestimated, which results in lower aerosol optical depth (AOD) values[20,21]. However, the AOD comparisons of two different runs with the absolute differences can help to offset the overestimation, and the relative differences may be overestimated due to underestimated AOD values. The considered SOA formation process can also contribute to the uncertainties, partly due to the complicated mechanism and partly due to the relatively simplified implementation in the large-scale model, as in TM5.

References

1 Li, X. & Xiao, J. Mapping Photosynthesis Solely from Solar-Induced Chlorophyll Fluorescence: A Global, Fine-Resolution Dataset of Gross Primary Production Derived from OCO-2. *Remote Sensing* **11**, 2563 (2019).

2 Zhu, Z. *et al.* Global Data Sets of Vegetation Leaf Area Index (LAI)3g and Fraction of Photosynthetically Active Radiation (FPAR)3g Derived from Global Inventory Modeling and Mapping Studies (GIMMS) Normalized Difference Vegetation Index (NDVI3g) for the Period 1981 to 2011. *Remote Sensing* **5**, 927-948 (2013).

3 Liu, Y. Y. *et al.* Recent reversal in loss of global terrestrial biomass. *Nature Climate Change* **5**, 470-474, doi:10.1038/nclimate2581 (2015).

4 Arneth, A. *et al.* Future vegetation–climate interactions in Eastern Siberia: an assessment of the competing effects of CO2 and secondary organic aerosols. *Atmos. Chem. Phys.* **16**, 5243-5262, doi:10.5194/acp-16-5243-2016 (2016).

5 Rantala, P., Aalto, J., Taipale, R., Ruuskanen, T. M. & Rinne, J. Annual cycle of volatile organic compound exchange between a boreal pine forest and the atmosphere. *Biogeosciences* **12**, 5753-5770, doi:10.5194/bg-12-5753-2015 (2015).

6 Schollert, M., Burchard, S., Faubert, P., Michelsen, A. & Rinnan, R. Biogenic volatile organic compound emissions in four vegetation types in high arctic Greenland. *Polar Biology* **37**, 237-249, doi:10.1007/s00300-013-1427-0 (2014).

7 Potosnak, M. J. *et al.* Isoprene emissions from a tundra ecosystem. *Biogeosciences* **10**, 871-889, doi:10.5194/bg-10-871-2013 (2013).

8 Angot, H. *et al.* Biogenic volatile organic compound ambient mixing ratios and emission rates in the Alaskan Arctic tundra. *Biogeosciences* **17**, 6219-6236, doi:10.5194/bg-17-6219-2020 (2020).

9 Tiiva, P. *et al.* Contribution of vegetation and water table on isoprene emission from boreal peatland microcosms. *Atmospheric Environment* **43**, 5469-5475, doi:https://doi.org/10.1016/j.atmosenv.2009.07.026 (2009).

10 Haapanala, S. *et al.* Measurements of hydrocarbon emissions from a boreal fen using the REA technique. *Biogeosciences* **3**, 103-112, doi:10.5194/bg-3-103-2006 (2006).

11 Holst, T. *et al.* BVOC ecosystem flux measurements at a high latitude wetland site. *Atmos. Chem. Phys.* **10**, 1617-1634, doi:10.5194/acp-10-1617-2010 (2010).

12 Seco, R. *et al.* Volatile organic compound fluxes in a subarctic peatland and lake. *Atmos. Chem. Phys.* **20**, 13399-13416, doi:10.5194/acp-20-13399-2020 (2020).

13 Eyring, V. *et al.* Overview of the Coupled Model Intercomparison Project Phase 6 (CMIP6) experimental design and organization. *Geosci. Model Dev.* **9**, 1937-1958, doi:10.5194/gmd-9-1937-2016 (2016).

14 Jokinen, T. *et al.* Production of extremely low volatile organic compounds from biogenic emissions: Measured yields and atmospheric implications. *Proceedings of the National Academy of Sciences* **112**, 7123-7128, doi:10.1073/pnas.1423977112 (2015).

15 Heinze, C. *et al.* ESD Reviews: Climate feedbacks in the Earth system and prospects for their evaluation. *Earth Syst. Dynam.* **10**, 379-452, doi:10.5194/esd-10-379-2019 (2019).

16 Lehsten, V., Mischurow, M., Lindström, E., Lehsten, D. & Lischke, H. LPJ-GM 1.0: simulating migration efficiently in a dynamic vegetation model. *Geosci. Model Dev.* **12**, 893-908, doi:10.5194/gmd-12-893-2019 (2019).

17 Scherrer, D., Vitasse, Y., Guisan, A., Wohlgemuth, T. & Lischke, H. Competition and demography rather than dispersal limitation slow down upward shifts of trees' upper elevation limits in the Alps. *Journal of Ecology* **108**, 2416-2430, doi:https://doi.org/10.1111/1365-2745.13451 (2020).

18 Soja, A. J. *et al.* Climate-induced boreal forest change: Predictions versus current observations. *Global and Planetary Change* **56**, 274-296, doi:https://doi.org/10.1016/j.gloplacha.2006.07.028 (2007).

19 Wolf, A., Callaghan, T. V. & Larson, K. Future changes in vegetation and ecosystem function of the Barents Region. *Climatic Change* **87**, 51-73, doi:10.1007/s10584-007-9342-4 (2008).

20 van Noije, T. P. C. *et al.* Simulation of tropospheric chemistry and aerosols with the climate model EC-Earth. *Geosci. Model Dev.* **7**, 2435-2475, doi:10.5194/gmd-7-2435-2014 (2014).

21 Aan de Brugh, J. M. J. *et al.* The European aerosol budget in 2006. *Atmos. Chem. Phys.* **11**, 1117-1139, doi:10.5194/acp-11-1117-2011 (2011).